Modulational instability regions for coupled Ginzburg-Landau equations with higher order of nonlinearities

Gholam-Ali Zakeri*
Department of Mathematics, and Interdisciplinary Research Institute for the Sciences (IRIS), California State University-Northridge, Northridge, California 91330-8313, USA

Emmanuel Yomba†
Department of Mathematics, California State University-Northridge, Northridge, California 91330-8313, USA

(Received 15 October 2014; published 4 June 2015)

A generalized (2+1)-dimensional coupled cubic-quintic Ginzburg-Landau equation with higher-order nonlinearities is fully investigated for modulational instability regions. We obtained the constraints that allow the modulational instability (MI) procedure to transform the system under consideration into an analysis of the roots of a polynomial equation of the fourth degree. Because of the complexity of the dispersion relation and its dependence on many parameters, we study numerous examples that are presented graphically. A numerical simulation based on a split-step Fourier method is implemented on the above equation. In addition to the general case, we have considered some special cases that allow us to investigate the behavior of MI in different regions.

DOI: 10.1103/PhysRevE.91.062904 PACS number(s): 05.45.Yv, 02.30.Hq, 02.30.Jr

I. INTRODUCTION

The complex Ginzburg-Landau equation (CGLE) is one of the most studied nonlinear equations in the physics community. It describes on a qualitative and often even on a quantitative level a vast variety of phenomena from nonlinear waves to second-order transitions and from superconductivity, superfluidity, and Bose-Einstein condensation (BEC) to liquid crystals, strings in field theory, and plasmas [1–5]. The generic equation and its different modifications [6–12] describe dissipative systems above the point of bifurcation. Dissipative systems are more complicated than Hamiltonian ones in the sense that, in addition to nonlinearity and dispersion, they include energy exchanged with an external source. Dissipative systems are common in nature. Observing nature, we can realize that "particles" are always submerged into dissipative media which feed their continuous motion [13]. Dissipative systems driven far from thermal equilibrium support soliton-like localized states. These structures are referred to as "dissipative solitons" [13]. Exact solutions for the cubic CGLE are available [14–16] but they are unstable.

The most straightforward modification of the model, which opens way to the stable solitary pulse, is the introduction of the cubic-quintic (CQ) nonlinearity, with linear gain and cubic loss in the cubic CGLE and an additional quintic loss that provides for the overall stability of the model. CQCGLE with higher-order terms has been also analyzed in the literature [17–19]. Other ways to try to stabilize the pulse is given in coupled CQCGLEs with a cross-phase modulation term; this extension includes spectra filtering gain, nonlinear gain, or absorption processes and higher-order correction to the nonlinear amplification or absorption and the intensity-dependent refractive index [20], where interpenetration, annihilation, and bound states of pulses could be accounted. One fundamental problem is to check the stability of the pulses, which is essential for the potential applications. Different kinds of instability may lead to phenomena such as phase turbulence, bistability, self-oscillation, and formation of static or moving patterns [21]. We note filamentation instability, solitary waves, and spatial chaotic patterns are the result of nonlinear development of modulational instability (MI) for unstable wave modes [22–25].

It is commonly known that a continuous wave (CW) is subject to MI under the effect of nonlinearity in combination with dispersion. In the MI process, weak perturbations imposed on a CW state grow exponentially due to the interplay between these nonlinear and dispersive effects. As time goes on, the modulation increases and CW breaks into a periodic pulse train [26]. MI is responsible for the formation of envelope solitons in electrical transmission lines [27–29]. The effect of MI is considered to be the main mechanism of rogue wave formation in all media. For example, it has been shown that MI can result in rogue formation in random wave fields [30]. Didenkulova *et al.* [31] demonstrated that MI can still play a significant role in the formation of rogue waves in the ocean for basins of 20 meters and large depth. For basins of small depth, the influence of MI is less probable. MI is an indispensable mechanism for the understanding of some relevant dynamical processes in BEC systems such as generation and propagation of solitary waves [32,33], matter-wave transport [34], and atomic number squeezing [35,36].

Recently, the study of MI in higher-order nonlinear Schrödinger (HNLS) equations has been done [37]. Mohamadou *et al.* [38] studied the effect of septic nonlinearity in the MI. The MI for NLSE with cubic-quintic nonlinearities and higher-order dispersion has been studied by Saha and Sarma [39]. The MI criterion for CGLE has been derived and investigated by Sabry *et al.* [40]. MI for the CGLE with higher-order terms has been studied by Mohamadou *et al.* [21]. MI in the CGLE with higher order, with fourth-order dispersion, and a cubic-quintic nonlinear term has been investigated by Tiofack *et al.* [41]. MI for coupled equations has been also studied by some authors. MI in the nonlinear optical coupler with negative-index metamaterial has been studied by Xiang

*ali.zakeri@csun.edu
†emmanuel.yomba@csun.edu

et al. [42]. MI in two cubic-quintic CGLE with a cross phase modulation type has been investigated in [43]. It is therefore, of interest to investigate MI in (2+1)-dimensional two cubic-quintic CGLE [44]. Such an investigation may throw new light onto better understanding of the formation of pulse on this system.

In the present paper, we study the derivation of the MI gain regions in the (2+1)-dimensional coupled CQCGLEs. This model is relevant to applications that the consideration of higher-order nonlinearities is important. We obtained the general roots of the dispersion relation. These equations describe the subcritical bifurcation to traveling waves. The paper is organized as follows: In Sec. II, we present the model that describes the complex Ginzburg-Landau equation with cubic-quintic terms. We obtained the set of constraints that allows us to have exact continuous-wave solutions. We performed linear stability analysis that leads to derivation of nonlinear dispersion equation. In Sec. II A we analyzed gain or loss and obtained a general requirement that allows the existence of the roots of the dispersion relation to facilitate the study of MI gain regions. In Sec. III, we report the results of numerous examples in the form of graphs that are classified into six groups. In Sec. III A, we present numerical simulations by allowing an initial perturbation into a regular soliton-like wave that resulted in a chaotic behavior. Section IV contains conclusions and final remarks. Finally, in the Appendix, we analyze some special cases that are offspring of the general case of Sec. II A.

II. MODEL AND LINEAR STABILITY ANALYSIS

The system of two coupled complex Ginzburg-Landau equations (CCGLEs) in (2+1)-dimension which arises as the envelope equations for a subcritical bifurcation to traveling waves could be written as follows [1]:

$$\partial_t A + v_g \partial_x A = \chi A + \gamma \nabla^2 A - \beta |A|^2 A - \delta |A|^4 A - \xi |B|^2 A, \tag{2.1}$$

$$\partial_t B - v_g \partial_x B = \chi B + \gamma \nabla^2 B - \beta |B|^2 B - \delta |B|^4 B - \xi |A|^2 B, \tag{2.2}$$

where the complex fields $A(x,y,t)$ and $B(x,y,t)$ are slowly varying envelopes and represent the right and left traveling waves. x and y are spatial variables and t is a temporal variable. Subscripts x and y denote the spatial derivatives. Subscript t denotes the temporal derivative. v_g is a real positive number representing the group velocity. χ is a real number representing the linear gain or loss. γ is a complex number representing the dispersion. β is a complex number representing the cubic nonlinearity. δ is a complex number representing the quintic nonlinearity. ξ is a complex number representing the coupling parameter. From here on, we write a complex number z as $z = z_r + iz_i$, where z_r denotes the real part and z_i denotes the imaginary part of z.

Equations (2.1) and (2.2) have the exact continuous-wave solutions in the forms of two plane waves,

$$A(x,y,t) = Me^{i(k_1 x + l_1 y - \omega_1 t)}, \tag{2.3}$$

$$B(x,y,t) = Pe^{i(k_2 x + l_2 y - \omega_2 t)}, \tag{2.4}$$

where $|M|$ and $|P|$ are positive real numbers representing the amplitudes of waves $A(x,y,t)$ and $B(x,y,t)$, respectively. k_1, k_2, l_1, and l_2 are real numbers representing the wave vectors. ω_1, and ω_2 are real numbers representing the angular frequencies.

We substitute the plane waves A and B given in Eqs. (2.3) and (2.4) into the system of the coupled CCQGLEs (2.1) and (2.2), require both imaginary and real parts to be zero, and solve step by step the four sets of equations to obtain the dispersion relations. It occurs that the plane waves A and B are the solutions of the system of the coupled CCQGLEs given in Eqs. (2.1) and (2.2) if the following dispersion relations are satisfied:

$$\omega_1 = \left(k_1^2 + l_1^2\right)\gamma_i + M^4\delta_i + M^2\beta_i + P^2\xi_i + k_1 v_g, \tag{2.5}$$

$$\omega_2 = \left(k_2^2 + l_2^2\right)\gamma_i + M^2\xi_i + P^4\delta_i + P^2\beta_i - k_2 v_g, \tag{2.6}$$

$$\left(k_1^2 + l_1^2\right)\gamma_r + \delta_r M^4 + M^2\beta_r + P^2\xi_r - \chi = 0, \tag{2.7}$$

$$\left(k_2^2 + l_2^2\right)\gamma_r + M^2\xi_r + \delta_r P^4 + P^2\beta_r - \chi = 0. \tag{2.8}$$

We note that the solution sets are functions of the system parameters and four arbitrary parameters.

The stability of the aforementioned solutions is analyzed by introducing the linear stability ansatz for the perturbed system (2.3) and (2.4),

$$A(x,y,t) = [M + \epsilon u(x,y,t)]e^{i(k_1 x + l_1 y - \omega_1 t)}, \tag{2.9}$$

$$B(x,y,t) = [P + \epsilon v(x,y,t)]e^{i(k_2 x + l_2 y - \omega_2 t)}, \tag{2.10}$$

where $u(x,y,t)$ and $v(x,y,t)$ are small perturbations of the carrier waves, i.e., both $|u(x,y,t)|$ and $|v(x,y,t)|$ are small compared to $|M|$ and $|P|$. Next, we substitute Eqs. (2.9) and (2.10) into Eqs. (2.1) and (2.2) and keep only the terms that are linear in $u(x,y,t)$ and $v(x,y,t)$, and we obtain two linearized equations

$$\begin{aligned} u_t + v_g u_x = {} & \gamma\nabla^2 u + 2i\gamma(k_1 u_x + l_1 u_y) - MP\xi(v + v^*) \\ & - M^2(\beta + 2\delta M^2)(u + u^*), \end{aligned} \tag{2.11}$$

$$\begin{aligned} v_t - v_g v_x = {} & \gamma\nabla^2 v + 2i\gamma(k_2 v_x + l_2 v_y) - MP\xi(u + u^*) \\ & - P^2(\beta + 2\delta P^2)(v + v^*), \end{aligned} \tag{2.12}$$

where * denotes complex conjugate. We assume general solutions of the form

$$u(x,y,t) = A_1 e^{i(Kx + Ly - \Omega t)} + A_2^* e^{-i(Kx + Ly - \Omega^* t)}, \tag{2.13}$$

$$v(x,y,t) = B_1 e^{i(Kx + Ly - \Omega t)} + B_2^* e^{-i(Kx + Ly - \Omega^* t)}, \tag{2.14}$$

where K and L are the wave numbers, Ω is the frequency of low-frequency perturbations modulating the carrier signal, and the parameters A_1, A_2, B_1, and B_2 are constant complex amplitudes. The substitution of Eqs. (2.13) and (2.14) into Eqs. (2.11) and (2.12) gives a linear homogeneous system of

equations in terms of A_1, A_2, B_1, B_2:

$$(n_{11}+i\Omega)A_1+n_{12}B_1+n_{13}A_2+n_{12}B_2=0, \quad (2.15)$$

$$n_{12}A_1+(n_{32}+i\Omega)B_1+n_{12}A_2+n_{34}B_2=0, \quad (2.16)$$

$$n_{21}A_1+n_{22}B_1+(n_{23}+i\Omega)A_2+n_{22}B_2=0, \quad (2.17)$$

$$n_{22}A_1+in_{42}B_1+n_{22}A_2+(n_{44}+i\Omega)B_2=0, \quad (2.18)$$

in which

$$\begin{aligned}
n_{11} &= \gamma^*(2k_1K+K^2+2l_1L+L^2)-iKv \\
&\quad +2M^4\delta^*+M^2\beta^*, \\
n_{12} &= MP\xi^*, \quad n_{13}=M^2(\beta^*+2M^2\delta), \\
n_{21} &= -M^2(\beta^*+2M^2\delta^*), \quad n_{22}=-MP\xi^*, \\
n_{23} &= \gamma^*(2k_1K-K^2+2l_1L-L^2)-iKv-2M^4\delta^*-M^2\beta^*, \\
n_{32} &= \gamma^*(2k_2K+K^2+2l_2L+L^2)+iKv+2P^4\delta^*+P^2\beta^*, \\
n_{34} &= P^2(\beta^*+2P^2\delta), \quad n_{42}=iP^2(\beta^*+2P^2\delta^*), \\
n_{44} &= \gamma^*(2k_2K-K^2+2l_2L-L^2)+iKv-2P^4\delta^*-P^2\beta^*.
\end{aligned}$$

Equations (2.15)–(2.18) constitute a system of four equations with four complex variables, i.e., $\mathbf{T}(A_1,B_1,A_2,B_2)=\mathbf{0}$ is a 4×4 complex matrix and $\mathbf{0}$ is the zero vector in C^4, Since we seek a nontrivial solution of $\mathbf{T}(A_1,B_1,A_2,B_2)=\mathbf{0}$, we require that $\mathrm{Det}\mathbf{T}=0$. After some straightforward calculations, we obtain the following nonlinear dispersion relation:

$$\Omega^4+C\Omega^3+D\Omega^2+E\Omega+F=0, \quad (2.19)$$

where

$$\begin{aligned}
C &= -(in_{11}+in_{23}+in_{32}+in_{44}), \\
D &= -\big(-n_{12}^2-2n_{22}n_{12}-n_{22}^2-n_{13}n_{21}+n_{11}n_{23}+n_{11}n_{32}+n_{23}n_{32}-in_{34}n_{42}+n_{11}n_{44}+n_{23}n_{44}+n_{32}n_{44}\big), \\
E &= -\big(-in_{21}n_{12}^2+in_{23}n_{12}^2+n_{42}n_{12}^2+in_{44}n_{12}^2+in_{11}n_{22}n_{12}-in_{13}n_{22}n_{12}-in_{21}n_{22}n_{12}+in_{22}n_{23}n_{12}+in_{22}n_{32}n_{12} \\
&\quad -in_{22}n_{34}n_{12}+n_{22}n_{42}n_{12}+in_{22}n_{44}n_{12}+in_{11}n_{22}^2-in_{13}n_{22}^2+in_{22}^2n_{32}+in_{13}n_{21}n_{32}-in_{11}n_{23}n_{32}-in_{22}^2n_{34}-n_{11}n_{34}n_{42} \\
&\quad -n_{23}n_{34}n_{42}+in_{13}n_{21}n_{44}-in_{11}n_{23}n_{44}-in_{11}n_{32}n_{44}-in_{23}n_{32}n_{44}\big), \\
F &= -\big(n_{11}n_{22}^2n_{32}-n_{13}n_{22}^2n_{32}-n_{12}n_{21}n_{22}n_{32}+n_{12}n_{22}n_{23}n_{32}-n_{11}n_{22}^2n_{34}+n_{13}n_{22}^2n_{34}+n_{12}n_{21}n_{22}n_{34}-n_{12}n_{22}n_{23}n_{34} \\
&\quad +in_{12}^2n_{21}n_{42}-in_{11}n_{12}n_{22}n_{42}+in_{12}n_{13}n_{22}n_{42}-in_{12}^2n_{23}n_{42}-in_{13}n_{21}n_{34}n_{42}+in_{11}n_{23}n_{34}n_{42}-n_{12}^2n_{21}n_{44} \\
&\quad +n_{11}n_{12}n_{22}n_{44}-n_{12}n_{13}n_{22}n_{44}+n_{12}^2n_{23}n_{44}+n_{13}n_{21}n_{32}n_{44}-n_{11}n_{23}n_{32}n_{44}\big).
\end{aligned}$$

The coefficients in Eq. (2.19) are complex and are functions of K, L, k_1, k_2, l_1, l_2, P, M, and the coefficients of Eqs. (2.1) and (2.2).

Remark. Observe that the MI procedure transforms the study of the system of the coupled CQCGLEs (2.1) and (2.2) into the analysis the roots of a polynomial of the fourth degree, given by Eq. (2.19).

A. Analysis of gain or loss

To investigate the gain or loss spectrum or the modulational instability regions, we must study the sign of the imaginary part of the roots of the dispersion equation (2.19). The dispersion equation has four roots given as follows:

$$\Omega_+^{\pm}=\pm\frac{1}{2}\sqrt{\frac{-C^3+4CD-8E}{4p_2}+\frac{3C^2}{4}-2D-p_2^2}-\frac{C}{4}+\frac{p_2}{2}, \quad (2.20)$$

$$\Omega_-^{\pm}=\pm\frac{1}{2}\sqrt{-\frac{-C^3+4CD-8E}{4p_2}+\frac{3C^2}{4}-2D-p_2^2}-\frac{C}{4}-\frac{p_2}{2}, \quad (2.21)$$

where

$$\begin{aligned}
p_2 &= \sqrt{\frac{C^2}{4}+\frac{-3CE+D^2+12F}{3p_1}-\frac{2D}{3}+\frac{p_1}{3}}, \\
p_1 &= 2^{-1/3}\sqrt[3]{p_0+27C^2F-9CDE+2D^3-72DF+27E^2}, \\
p_0 &= \sqrt{(27C^2F-9CDE+2D^3-72DF+27E^2)^2-4(-3CE+D^2+12F)^3}.
\end{aligned}$$

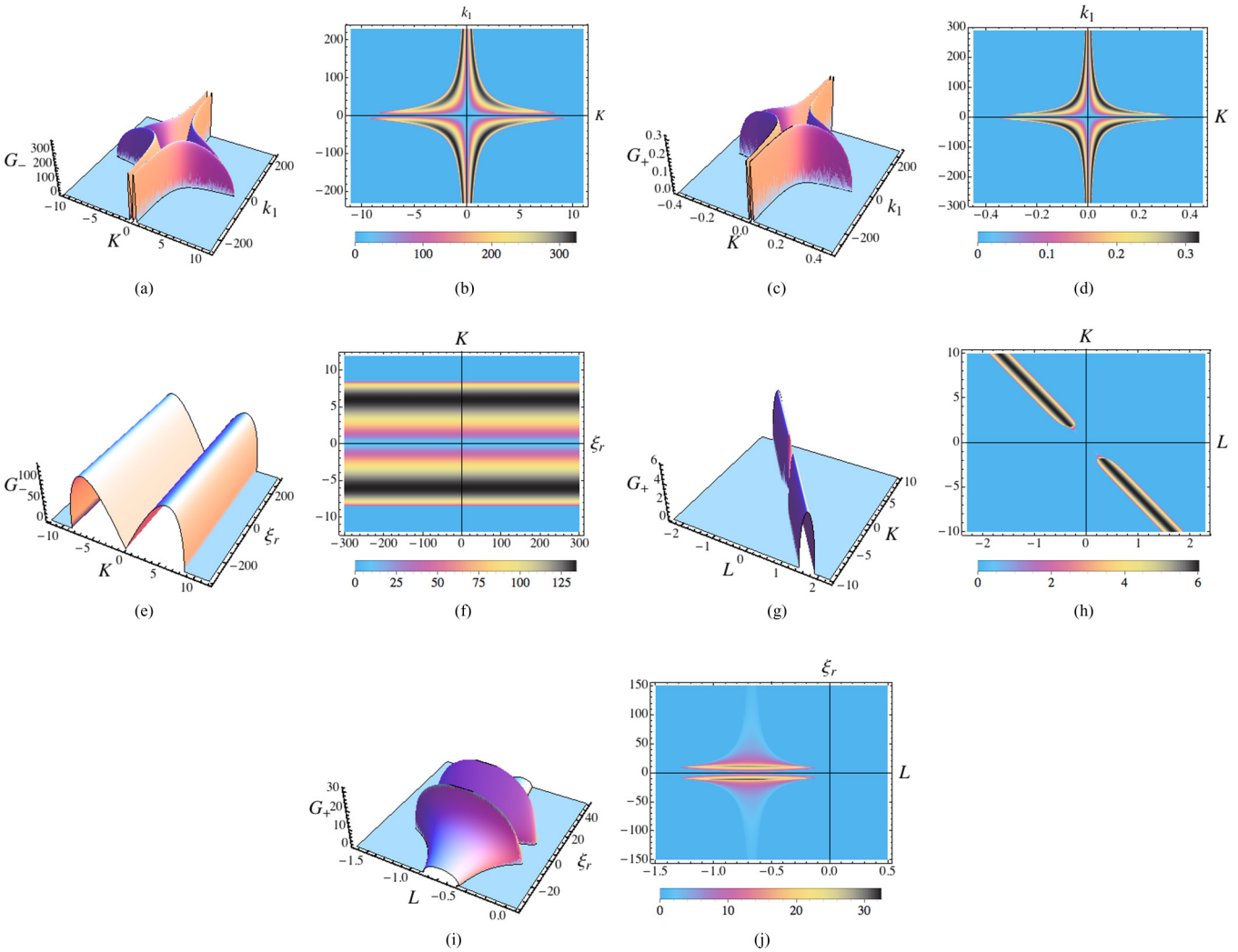

FIG. 1. (Color online) Regions of MI illustrating finite gain over unbounded regions associated with solutions G_+ and G_- of Eq. (A2), where K and L are the wave numbers of perturbed waves, and k_1 is the wave number of the continuous wave and ξ_r is the real part of coupling parameter. Plots (a), (c), (e), (g), and (i) show the finite gain of MI, and their corresponding density plots (b), (d), (f), (h), and (j) show the regions where gains occur. All plots given here exhibit a symmetry.

The quantities $\Omega_\pm^\pm$ depend on the values of the parameters given in the coefficients of the dispersion relation. The spectrum gain $G(K,L)$ can be a positive or a negative number. For a given set of parameters and for a particular set of values of the wave numbers, we can specify its sign. Negative value indicates the growth rate $\mathrm{Im}(\Omega_\pm^\pm)$ which means the stability of the system because of the vanishing long term of $\exp[\mathrm{Im}(\Omega_\pm^\pm)t]$ as $t \to \infty$. In this case, the system remains stable under modulation, while its positive values are signature of instabilities. The perturbation diverges without limit as time t increases and the corresponding solution is said to be modulationally unstable. So the signs of $\mathrm{Im}(\Omega_\pm^\pm)$ determine the stability of the solution of the system of the coupled CCQGLEs. The regions of instability are called MI gain spectrums and are regions where the gain $G_1 = 2\mathrm{Im}(\Omega_-^-) > 0$, or $G_2 = 2\mathrm{Im}(\Omega_-^+) > 0$, or $G_3 = 2\mathrm{Im}(\Omega_+^-) > 0$, or $G_4 = 2\mathrm{Im}(\Omega_+^+) > 0$ occur.

The above roots given by Eqs. (2.20) and (2.21) exist whenever $p_1 \neq 0$ and $p_2 \neq 0$. If $p_1 = 0$ then we must have $D^2 - 3CE + 12F = 0$. Under this condition, $p_2 = 0$ reduces to $C^3 - 4CD + E = 0$ (and $C \neq 0$ or $E \neq 0$). Note that these expressions appear, for example, in p_2 and Eq. (2.20). Thus the above roots exist whenever $(D^2 - 3CE + 12F)(C^3 - 4CD + E) \neq 0$. This indicates that the special case where $C = E = 0$ must be considered separately. The coefficients of Eq. (2.19) are very complicated because each coefficient depends on many parameters. In the Appendix, we consider the case where $CE = 0$. Using the results obtained in Eqs. (2.20) and (2.21) and those given in the Appendix, we have performed numerous examples to analyze the effects of the parameters on the stability of the perturbed plane waves A and B given by Eqs. (2.9) and (2.10) as discussed in the next section. We conclude this section with the following result:

Theorem: The system of two coupled complex Ginzburg-Landau equations (2.1) and (2.2) has a nonlinear dispersion equation given by Eq. (2.19) with four roots given by Eqs. (2.20) and (2.21) subject to $(D^2 - 3CE + 12F)(C^3 - 4CD + E) \neq 0$ and at least one of C or E is nonzero.

III. GAIN OR LOSS REGIONS

To describe regions where modulational instabilities occur for the roots of Eq. (2.19) obtained in the pervious section, we consider plots for $G_- = 2\mathrm{Im}[\Omega_-^-]$ and $G_+ = 2\mathrm{Im}[\Omega_+^+]$. To understand the role played by nonlinearity in modulational instability we use the following parameter values and constraint conditions associated with each case. For all cases we use the following values for $v_g = 0.75$, $\epsilon = 0.5$, $\beta = 2.2 + 2.6i$, $\gamma = -0.01 + i$, $\delta = 0.8 - i$, $k_2 = 0.8$, $l_1 = 7$, $l_2 = 9$, and $\xi = 3 - 2i$. Figures 1(a)–1(d) and 10(a) are plotted using the above data values and the relations given in case 1.2. Figures 1(e), 1(f), 1(i), 1(j), 2(a), 2(b), 2(e), and 2(f) are plotted using the additional data values given by $\xi = -2$, $k_1 = 7$, $k_2 = 0.8$, $l_1 = 8$, and $l_2 = 9$ and the relations given in case 1.2. Figures 2(c) and 2(d) are plotted using data values $l_1 = -l_2 = 7$, $K = 4$, and $k_1 = -k_2 = 0.8$ and the relations in case 1.2. Plots given in Figs. 1(g), 1(h), 7(a) and 7(b) are obtained using $\chi = 1.5$, $\gamma = i$, $\xi = 0.8$ and the relations in case 1.3. Using the above data values and the relations in case 1.4, we obtained Figs. 3(a) and 3(b). Relations in case 1.5

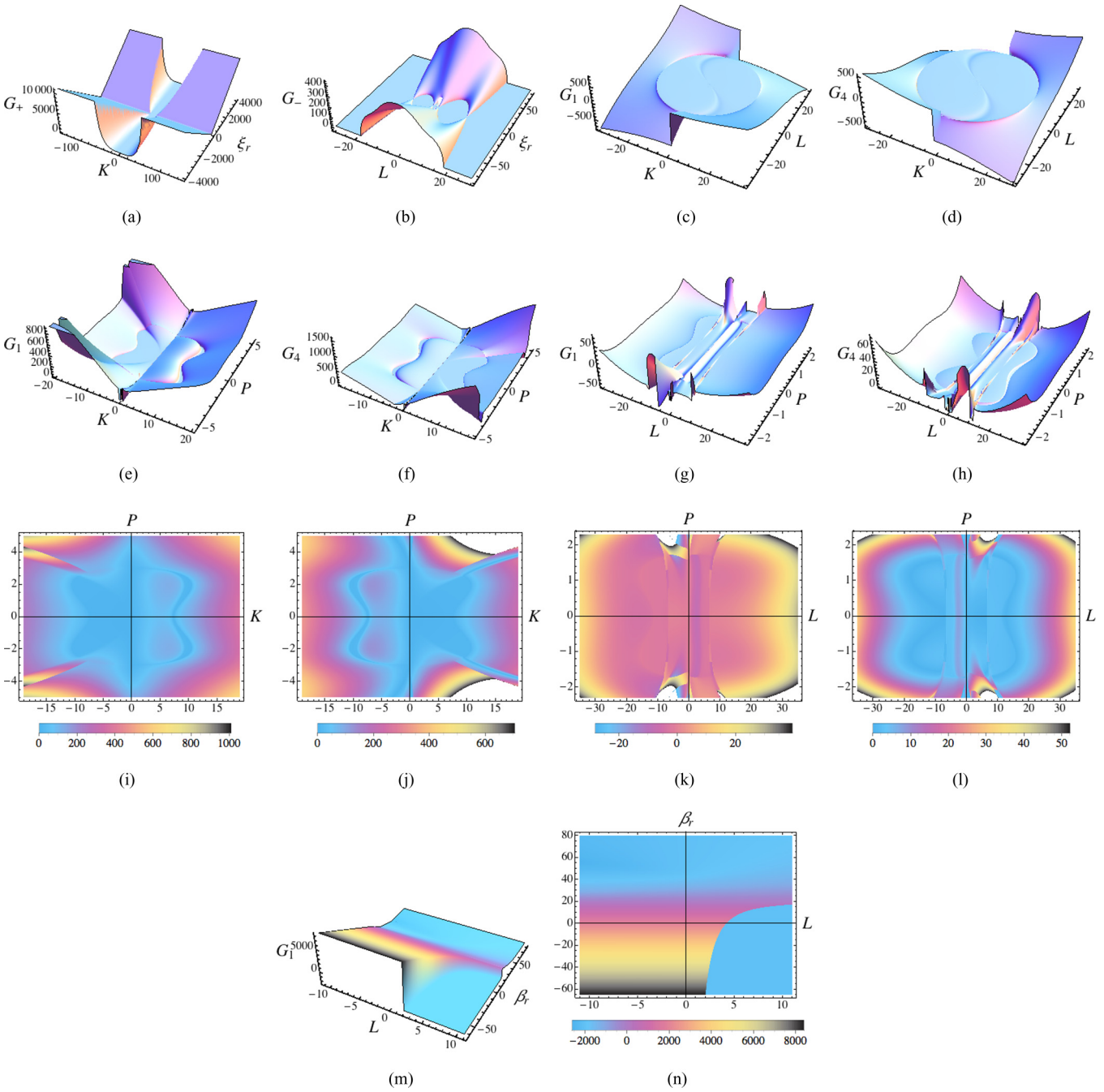

FIG. 2. (Color online) Regions of MI gains illustrating unbounded gains over unbounded regions associated with solutions G_+ and G_- of Eq. (A2), and $G_1 - G_4$ of Eqs. (2.20) and (2.21), where K and L are the wave numbers of perturbed waves, P is the amplitude of the continuous wave and ξ_r, β_r are both the real parts of coupling and cubic nonlinear terms, respectively. Panels in (a)–(h) and (m) show unbounded gains of MI, and the corresponding density plots for (e)–(h) and (m) are given in (i)–(l) and (n), respectively.

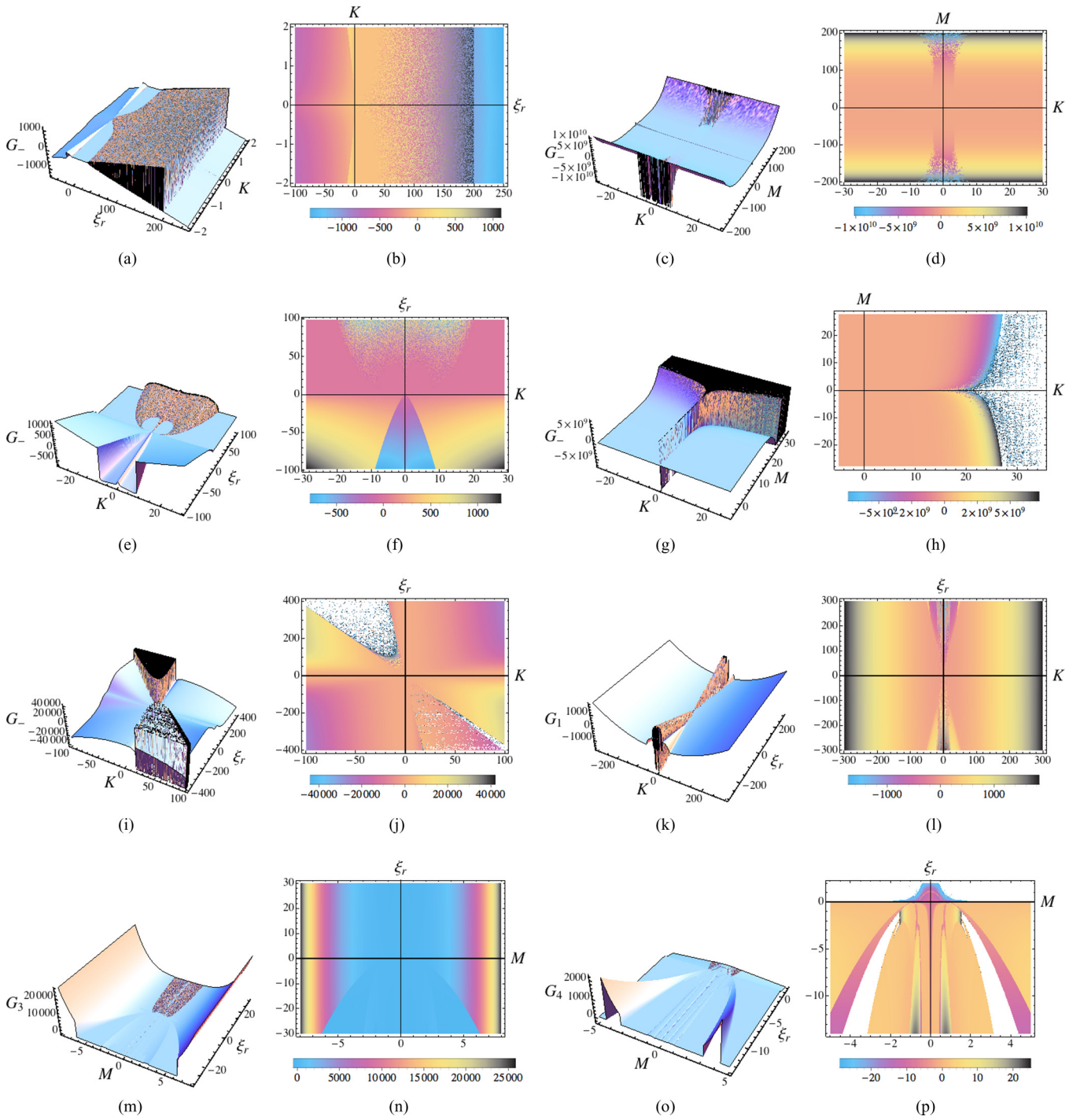

FIG. 3. (Color online) Regions of MI illustrating unbounded gains over unbounded regions associated with solutions G_- of Eq. (A2), and $G_1 - G_4$ of Eqs. (2.20) and (2.21), where K is the wave number of perturbed wave, M is the amplitude of the continuous wave, and ξ_r is the real part of the coupling term. Panels in (a), (c), (e), (g), (i), (k), (m), and (o) show unbounded gains of MI, and their corresponding density plots are in (b), (d), (f), (h), (j), (l), (n), and (p), respectively. The spiky regions in each plot are the chaotic regions.

are used to plot Figs. 10(b) and 7(s). We used the relations in case 1.7 and the data values $\xi = 3.2 - 2i$, $k_1 = 8$, $k_2 = 10$, $K = 10$, $P = 1.5$, and $M = 2$ for obtaining plots in Figs. 7(c) and 7(d). For generating plots in Figs. 4(c) and 4(d) we used the relations given in case 1.7 with additional data values $\chi - 0.15, \epsilon = 0.05, \xi = 0.32 - 0.2i$, and $\delta = 0.08$. For plots in Figs. 2(e)–2(p) we used the relations in case 2.1 and the additional data values $\beta = 1.2 - i, \delta = -0.8 - i, \epsilon = 0.3$, $\xi = 0.04 + 2i$, $P = \epsilon M$, $\chi = -0.01$, and $\gamma = 0.01 + i$. For the rest of figures, we used the general case formulation of Sec. II A, and cases 1.6, 2.2, and 2.3. We have classified our plots into the following groups:

(i) Unbounded MI gain regions with finite gains without chaotic regions (Fig. 1).

(ii) Unbounded MI gain regions with unbounded gains without chaotic regions (Fig. 2).

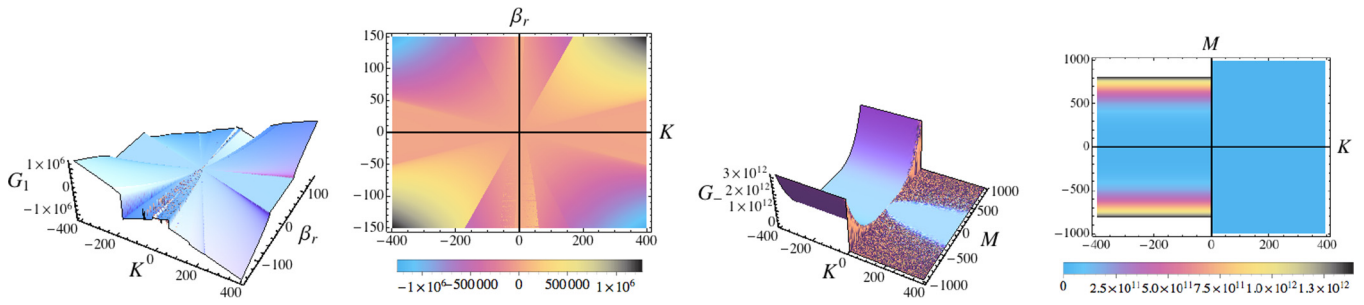

FIG. 4. (Color online) Regions of MI illustrating unbounded gains over unbounded regions with unstable regions are associated with solutions G_- of Eq. (A2), and G_1 of Eq. (2.21), where K is the wave number of the perturbed wave, M is the amplitude of the continuous wave, and β_r is the real part of the cubic nonlinear term. Plots (a) and (c) show unbounded gains of MI, and their corresponding density plots (b) and (d) show the regions where gains occur. All plots given here present a symmetry. The spiky region in each plot indicates the chaotic region.

(iii) Unbounded MI gain regions with unbounded gains that include chaotic regions (Figs. 3 and 4).

(iv) Bounded MI gain regions with finite gains with chaotic regions (Fig. 5).

(v) Bounded MI gain regions with finite gains in a mostly chaotic regions (Fig. 6).

(vi) Bounded MI gain regions with finite gains without chaotic regions (Fig. 7).

Figure 1 describes unbounded regions of modulation instabilities with finite gains and their corresponding density plots associated with each plot. Figures 1(a) and 1(c) show variations of k_1 and K on MI and illustrate two waves moving along the K axis in the neighborhood of $k_1 = 0$ and moving forward with increasing amplitude, and as they are approaching $K = 0$ they move apart then reflect on the positive side of the K axis and move forward as illustrated. In this case, G_- has a much larger gain than G_+. Figure 1(e) shows the variation of ξ_r and K creating an M-shaped wave moving along the K axis. Figure 1(g) shows the variation of L and K having an up-down U-shaped wave form in the neighborhood of the origin split and moves along the line $K = -L$ away from the origin. Figure 1(i) shows the variation of $G_+(L,\xi_r)$. All plots in this figure are symmetric with respect to some axis.

Using the same data values as before, in Fig. 2 we provide a group of plots that have unbounded regions of MI with unbounded gains. Figures 2(a) and 2(b) show solutions of Eq. (A2) for $G_+(K,\xi_r)$ and $G_-(L,\xi_r)$, respectively. In these plots we used the constraints imposed on case 1.2 in the Appendix, which uses the assumption that $CE = 0$. Figures 2(c) and 2(d) illustrate solutions of Eq. (2.20) for G_1 and G_4 as functions of (K,L), respectively. Figures 2(e)–2(h) illustrate solutions of Eq. (2.20) as functions of K and P using the general case with the assumption that $CE \neq 0$ with their corresponding density plots in Figs. 2(i)–2(l). Figure 2(m) describes the solution of Eq. (2.20) as a function of L and β_r under the assumption of $CE \neq 0$ with its corresponding density plot in Fig. 2(n).

Figure 3 shows a collection of plots with chaotic regions. Again all plots have some geometrical symmetries. The plots in Fig. 3 were very time consuming to obtain. For example, the CPU time for the plot in Fig. 3(a) was over 2 h using an OS X processor 2.8-GHz Intel Core i7 with a 16-GB memory, 1600 MHz DDR3. The chaotic regions in the plots of Figs. 3(a)–3(p) are shown as spiky or dotted regions in their density plots. Except for Fig. 3(a), the rest of the plots in this figure exhibit unbounded regions of MI with unbounded gains. The chaotic regions for Figs. 3(a), 3(m), and 3(o) have finite oscillations, while the rest of plots in this figure have infinite oscillations.

Figure 4 shows plots with mild chaotic regions with small variation. Figure 4(a) shows the variation of K vs β_r using data values as in Fig. 1 and $CE \neq 0$. Figure 4(c) uses case 2.1 relations. In both these plots, we have examples of unbounded regions of MI with unbounded gain and a chaotic region with small variations.

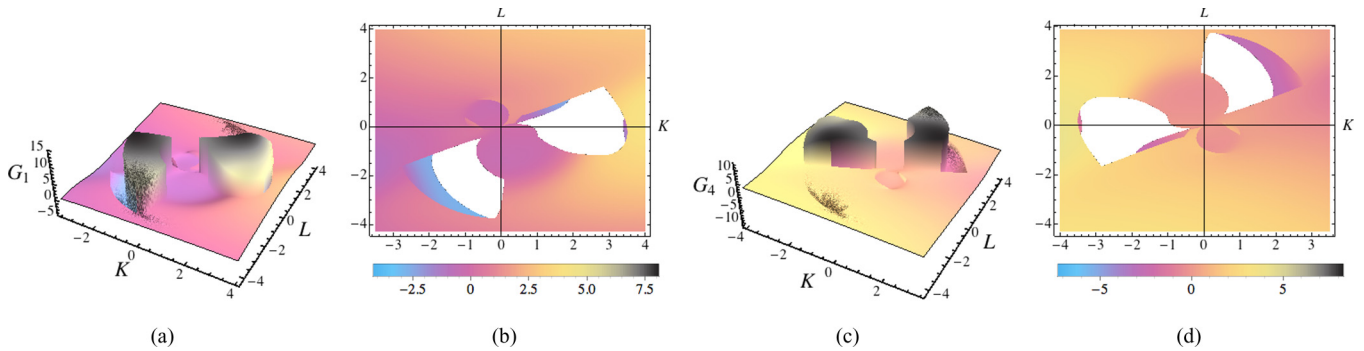

FIG. 5. (Color online) Regions of MI illustrating local gains over bounded regions with unstable regions are associated with solutions G_1 and G_4 of Eqs. (2.20)–(2.21), where K and L are the wave numbers of the perturbed waves. The spiky region in each plot indicates chaotic region.

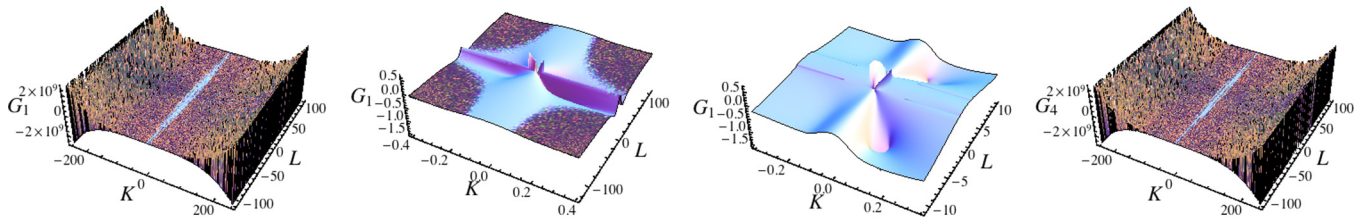

FIG. 6. (Color online) Plots of solutions G_1 and G_4 of Eqs. (2.20) and (2.21) exhibit a chaotic behavior almost everywhere, where K and L are the wave numbers of perturbed waves. Plots (b) and (c) are the zoomed portions at the origin of plot (a). Plot (c) shows small gains at the origin for small values of K and L. The spiky region in each plot indicates a chaotic region. Large oscillations occur for relatively large values of K.

The plots in Fig. 5 show MI with small gain only over a bounded region with minor chaotic activity. No geometrical symmetries are observed in this case. The plots were obtained under the assumption that $CE \neq 0$ with same data values as in Fig. 1.

Figures 6(a) and 6(d) show examples of solutions that are almost chaotic except over a very small region. Figures 6(b) and 6(c) are zoomed versions of Fig. 6(a) near the origin. Plots were obtained under the assumption that $CE \neq 0$.

Panels in Fig. 7 illustrate finite MI gains over bounded regions without any chaotic behaviors. Figure 7(a) shows two circular waves colliding along the line $K = -0.1L$, and at the point of collision the maximum MI gain is observed. Fig. 7(a) was obtained using case 1.3 constraints. Figures 7(a) and 7(c) were obtained using $CE = 0$ and the rest under the assumption that $CE \neq 0$.

In Fig. 8, we present solutions of Eq. (A2) under the assumption obtained under the case 1.7 stated in the Appendix. This figure illustrates the MI for unbounded gains over unbounded regions with some chaotic regions. In Fig. 9, we present cross-sections of some of MI gains associated with Eq. (A2). In Fig. 10, we present solutions of Eqs. (A2) and (2.20) of MI gains in the neighborhood of the origin.

A. Numerical simulations

In this section we consider a direct numerical simulation of the system of equations in Eqs. (2.1) and (2.2). We introduce a small initial modulational perturbation to continuous-wave states with the objective of identifying nonlinear patterns generated by the modulation instabilities. Following [26] we consider a signal in the form of

$$\begin{aligned} A(x,y,0) &= M[1 + A_m \sin(2\pi\Omega_{1m}x + 2\pi\Omega_{2m}y)] \\ &\quad \times e^{-i\omega_{11}x - i\omega_{12}y}, \\ B(x,y,0) &= P[1 + B_p \sin(2\pi\Omega_{1p}x + 2\pi\Omega_{2p}y)] \\ &\quad \times e^{-i\omega_{21}x - i\omega_{22}y}, \end{aligned}$$

where A_m and B_p are modulation amplitudes, and Ω_{1m}, Ω_{2m}, Ω_{1p}, and Ω_{2p} are the frequencies of weak sinusoidal modulations imposed on the continuous waves in the x and y directions, respectively. We use the split-step Fourier method to solve Eqs. (2.1) and (2.2) subject to the initial conditions given above.

The main idea behind this method is to obtain an approximate solution by assuming that for the wave solution over a small Δt, the dispersive and nonlinear effects act independently. That is, the propagation of the wave solution from t to $t + \Delta t$ is carried out in two steps. In the first step, the nonlinearity acts alone, and in the second step, dispersion acts alone. That is, Eqs. (2.1) and (2.2) are written as

$$\partial_t A = (-\chi - \gamma\nabla^2 - v_g\partial_x)A + (-\beta|A|^2 - \delta|A|^4 - \xi|B|^2)A,$$

$$\partial_t B = (-\chi - \gamma\nabla^2 + v_g\partial_x)B + (-\beta|B|^2 - \delta|B|^4 - \xi|A|^2)B.$$

Here, in each equation, the first parenthesis represents the differential operator that accounts for dispersion and absorption in a linear medium and the second parenthesis is a nonlinear operator that governs the nonlinearities in pulse propagation. Thus, the above equations can be rewritten briefly as

$$\partial_t A = \widehat{D}_1 A + \widehat{N}_1 A,$$

$$\partial_t B = \widehat{D}_2 B + \widehat{N}_2 B,$$

where $\widehat{D}_1$ and $\widehat{D}_2$ are the operators for dispersion and absorption in the linear medium and $\widehat{N}_1$ and $\widehat{N}_2$ are the nonlinear operators for pulse propagation as defined by the model equations.

Then, to improve the accuracy of the standard split-step Fourier method over one segment from t to $t + \Delta t$, we adopted the following procedure to propagate the wave:

$$\begin{aligned} A(x,y,t+\Delta t) \approx \exp\left(\Delta t \int_t^{t+\Delta t} \widehat{D}_1(x,y,t')dt'\right) \\ \times \exp(\Delta t \widehat{N}_1)A(x,y,t), \end{aligned}$$

and similarly for $B(x,y,t+\Delta t)$. We approximated the integrals in the above expression by using the composite trapezoidal rule of two subdivisions to increase the accuracy of the result. We let $A_m = 0.001$, $B_p = 0.002$, $\Omega_{1m} = \Omega_{2m} = 0.5$, $\Omega_{1p} = \Omega_{2p} = 0.43$, $\omega_{11} = \omega_{12} = 0.3$, $\omega_{21} = \omega_{22} = 0.41$, $v_g = 0.75$, $\chi = 0.6$, $\gamma = -0.01 + i$, and $\xi = 0.56$.

We consider a simulation of Eqs. (2.1) and (2.2) to study the evaluation of the amplitude of a continuous wave with and without the presence of nonlinearity. In particular, we want to consider the competing effect of cubic and quintic terms. To ensure the accuracy of our numerical results by lessening the influence of the error due to the computational boundary of the regions, the spatial grid was chosen sufficiently large to prevent problems from boundary of the regions [26]. Running various numerical examples we note that when $|\beta| \leqslant |\delta|$ then

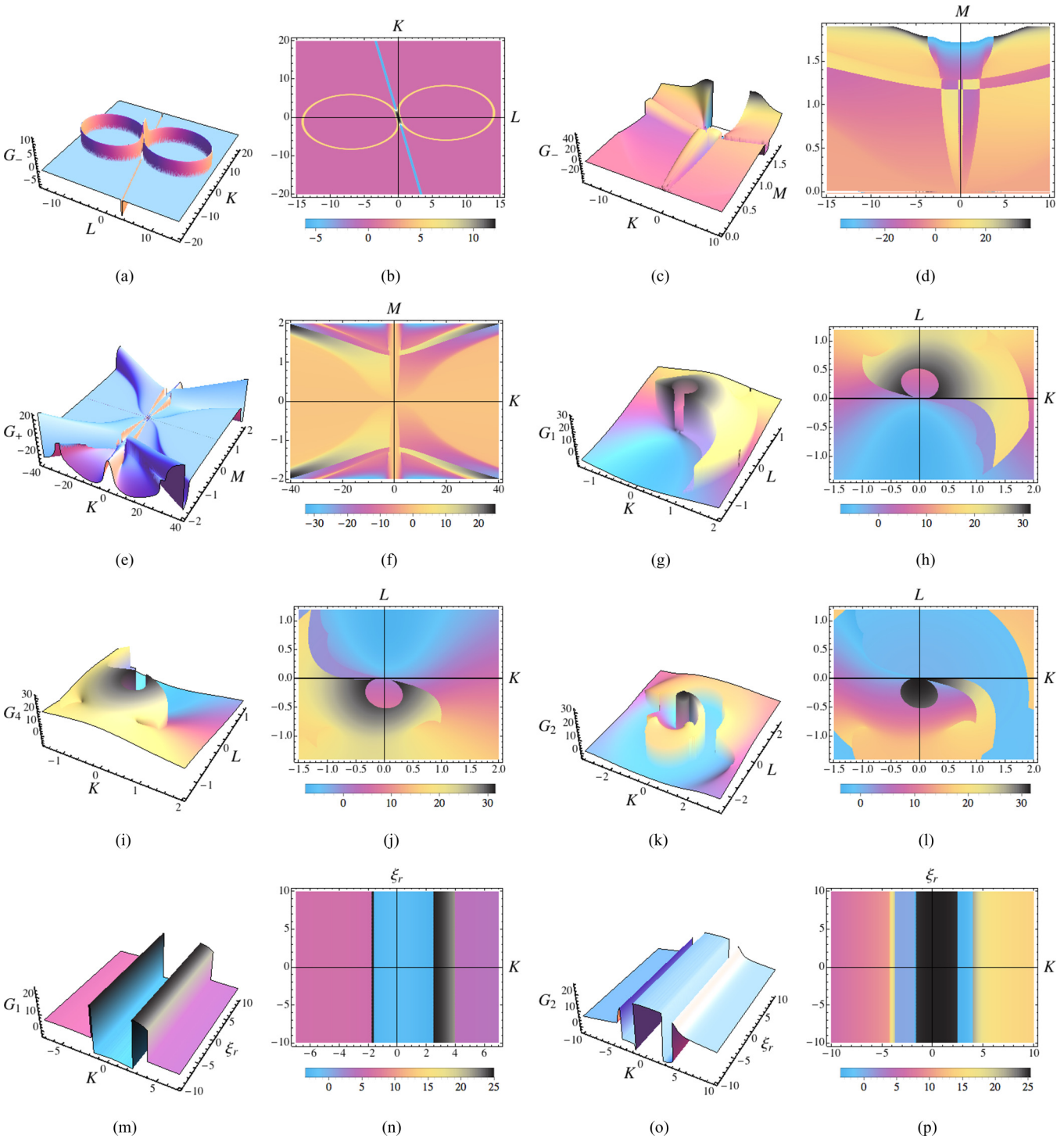

FIG. 7. (Color online) Regions of MI illustrating finite gains over bounded regions associated with solutions G_-, G_+ of Eq. (A2), and $G_1 - G_4$ of Eqs. (2.20) and (2.21), where K, L, are wave numbers of the perturbed waves, M, P are amplitudes of continuous waves, and ξ_r is the real part of the coupling term. Plots (a), (c), (e), (g), (i), (k), (m), and (o) show finite local gains of MI, and their corresponding density plots in (b), (d), (f), (h), (j), (l), (n), and (p) show the regions where gains occur.

the outcome is the generation of a periodic train of solitary pulses. However, when $|\beta| > |\delta|$ then the continuous wave turns progressively to a chaotic train of solitary pulses. This result is in agreement with the conclusion given in [45].

Figure 11 shows how evolution of a continuous wave progressively turns into a chaotic mode for amplitude as a function of (x,t) when y is kept fixed. In Figs. 11(a)–11(c), the strength $|\beta|$ of the cubic nonlinearity is increased while we kept the magnitude of strength of the quintic nonlinearity $\delta = 0.8 - i$ fixed. Figures 12(a) and 12(b) show the evolution of a continuous wave when the strength of the cubic term is slightly larger than the strength of the quintic term; the solution after some time becomes chaotic. Figure 12(c) is a snapshot of amplitude $|A(x,y,c)|$ when t is fixed. In Figs. 11(a)–11(c)

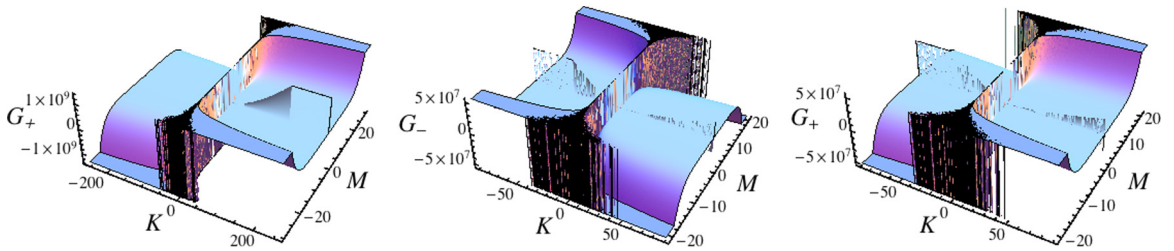

(a) (b) (c)

FIG. 8. (Color online) MI for unbounded gains over unbounded regions with some chaotic regions for solutions of G_-, G_+ of Eq. (A2) using case 1.7 stated in the Appendix. The spiky region in each plot is the chaotic region.

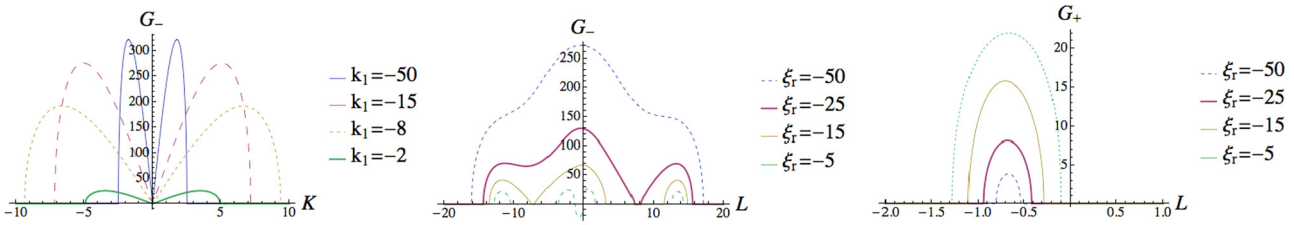

(a) (b) (c)

FIG. 9. (Color online) Plots of MI gains associated with solutions G_-, G_+ of Eq. (A2). Panels in (a), (b), and (c) are related to Figs. 1(a), 2(c), and 1(i), respectively.

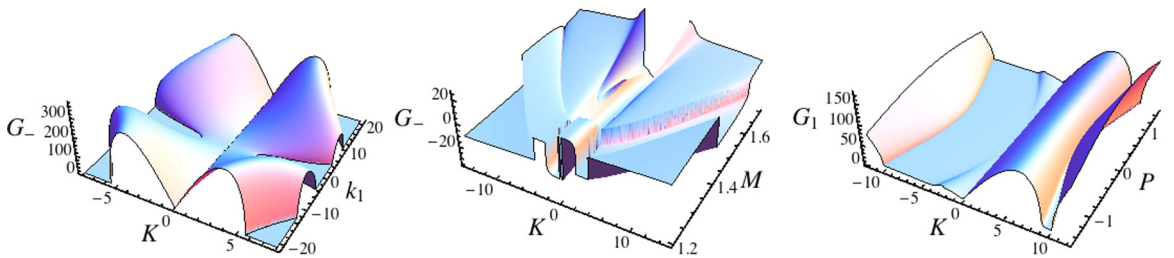

(a) (b) (c)

FIG. 10. (Color online) Regions of MI gains for solutions G_- of Eq. (A2) and G_1 of Eq. (2.20). Panels in (a), (b), and (c) are related to zoom portion of plots in Figs. 1(a), 3(c), and 2(k), respectively.

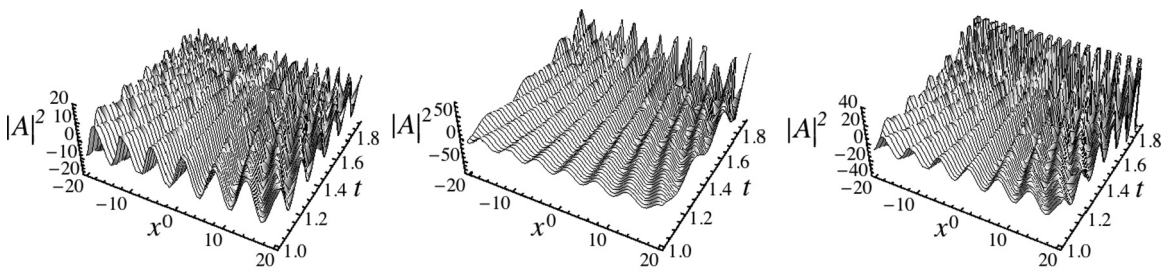

(a) $\beta = 0.8 + 1.2i$ (b) $\beta = 1.2 + 1.6i$ (c) $\beta = 2.2 + 2.6i$

FIG. 11. Evolution of a plane wave with initial perturbation by a weak sinusoidal wave leading to chaotic behavior when the strength of the cubic nonlinearity is more than the strength of the quintic nonlinearity, $|\beta| > |\delta|$, for $\delta = 0.8 - i$. Plots for $|B|^2$ are similar to (a)(c). We have let $y = 0$.

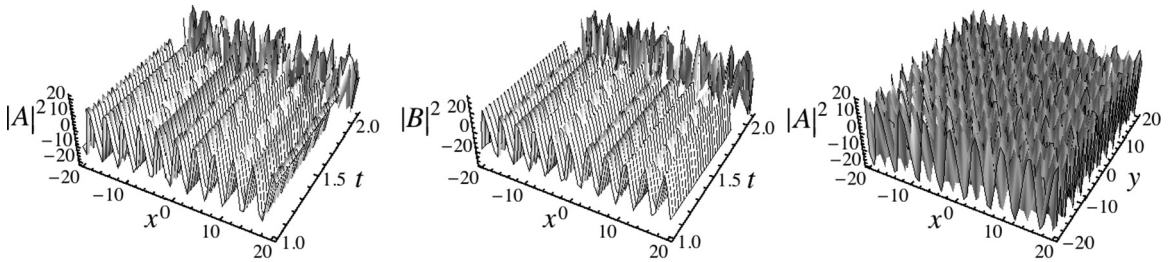

FIG. 12. Panels (a) and (b) show the evolution of a plane wave leading to chaotic behavior when the strength of cubic nonlinearity is slightly more than the strength of quintic nonlinearity, $|\beta| > |\delta|$, for $\beta = 0.8 - 1.01i$, $\delta = 0.8 - i$, and $y = 0$. Plots for $|A(c,y,t)|^2$ and $|B(c,y,t)|^2$ when x is fixed are similar to (a) and (b). Panel (c) shows a snapshot of amplitude magnitudes for a continuous wave as function of x, y at time $t = 2.1$.

and in Figs. 12(a) and 12(b) we kept y fixed to plot the magnitudes of the amplitudes. The plots of amplitude magnitudes when x is kept constant are similar to those in Figs. 11 and 12. The chaotic behavior shown in the Figs. 11 and 12 is not surprising because we know from the literature that the cubic Ginzburg-Landau equation (GLE) [46,47], the cubic-quintic GLE [48,49], and the coupled GLEs [50] exhibit spatiotemporal chaos (when driven away from equilibrium, spatially extended systems can exhibit irregular behavior in space and time; this phenomenon is commonly referred to as spatiotemporal chaos [46]).

IV. CONCLUSIONS AND FINAL REMARKS

A generalized (2+1)-dimensional coupled cubic-quintic Ginzburg-Landau equation with higher-order nonlinearities was investigated for the existence of modulational instability regions. We obtained a nonlinear dispersion relation as a fourth-degree polynomial with complex-valued coefficients. General roots of this equation were analyzed by considering gain spectrums of modulational instability expression as twice the imaginary part of each root of dispersion equation. Because of the complexity of the roots, we imposed a set of constraints that allows us to investigate modulational instability regions. Dispersion relation depends on several parameters; thus for better understanding of the behavior of solutions, we performed numerous examples and we presented the results graphically.

Our results are classified into six subclasses: (i) unbounded MI gain regions with finite gains without chaotic regions, (ii) unbounded MI gain regions with unbounded gains without chaotic regions, (iii) unbounded MI gain regions with unbounded gains that include chaotic regions, (iv) bounded MI gain regions with finite gains with chaotic regions, (v) bounded MI gain regions with finite gains in a mostly chaotic regions, and (vi) bounded MI gain regions with finite gains without chaotic regions.

We have shown from cases 1.1–1.4 stated in the Appendix that when keeping all parameters fixed, then as the real part of quintic nonlinearity increases the waves amplitudes and the coefficient of linear gainor loss decrease. We obtained conditions under which the dispersion equation (2.19) has valid solutions for the general case. In addition to the general case, we also considered some special cases that allowed us to investigate the behavior of MI in different regions. A numerical simulation that is based on a split-step Fourier method was used to investigate the perturbed associated problem. Performing various numerical examples we noted that when $|\beta| \leqslant |\delta|$, then the outcome is the generation of a periodic train of solitary pulses. However, when $|\beta| > |\delta|$, the obtained train of solitary pulses exhibits chaotic behavior. The method used in this paper can be applied to a large class of generalized Korteweg–de Vries equations given in [51].

ACKNOWLEDGMENTS

The authors are grateful to the referees for their constructive criticisms and comments that improved the presentation of the manuscript.

APPENDIX

The roots of the dispersion relation given by Eq. (2.19) for the general case are given by Eqs. (2.20) and (2.21). In Sec. II A, we showed that the roots of the dispersion relation exist if $(D^2 - 3CE + 12F)(C^3 - 4CD + E) \neq 0$ and at least one of C or E is nonzero. In this section we analyze the behavior of the roots of the dispersion equation under the assumption that $CE = 0$. This assumption leads to three cases that are discussed below. For the sake of simplicity of notation, we define a non-negative function that depends on the real parts of the six parameters in the coupled CQCGLE equations and the two continuous-wave amplitudes as follows.

Definition. The real-valued *wave-vector component function* for the system of two coupled complex Ginzburg-Landau equations (2.1) and (2.2) having continuous-wave solutions (2.3) and (2.4) is given by

$$\phi(M,P,k_1) = \sqrt{\frac{\chi - k_1^2\gamma_r - M^4\delta_r - M^2\beta_r - P^2\xi_r}{\gamma_r}}. \quad \text{(A1)}$$

Case 1. $C = E = 0$. Let us first consider the special case when $C = E = 0$, reducing Eq. (2.19) to

$$\Omega^4 + D\Omega^2 + F = 0. \quad \text{(A2)}$$

The roots of Eq. (A2) are determined explicitly. Their expressions are given as

$$\Omega_+^{\pm} = \pm 2^{-1/2}\sqrt{-D + \sqrt{D^2 - 4F}},$$
$$\Omega_-^{\pm} = \pm 2^{-1/2}\sqrt{-D - \sqrt{D^2 - 4F}}. \quad \text{(A3)}$$

The values of $\Omega_{\pm}^{\pm}$ depend upon the values of the parameters in the coefficients of the dispersion relation. The sign of $\mathrm{Im}(\Omega_{\pm}^{\pm})$ determines the stability of the continuous-wave solutions of the system of the coupled CQCGLE equations given by Eqs. (2.1) and (2.2). We study the dependence of the imaginary parts of the roots of the dispersion relation given by Eq. (A3). The constraint conditions $C = 0$ and $E = 0$ give four additional equations upon expanding these quantities and setting real and imaginary of each equal to zero. We must select the parameters so that these four constraints together with the two constraints given in Eqs. (2.7) and (2.8) hold true. These constraints help us to select four arbitrary parameters among the ten parameters we have in this problem. These relations are as follows:

$$\begin{aligned}
\gamma_r\left(k_1^2+l_1^2\right)+M^4\delta_r+M^2\beta_r+P^2\xi_r-\chi&=0,\\
\gamma_r\left(k_2^2+l_2^2\right)+M^2\xi_r+P^4\delta_r+P^2\beta_r-\chi&=0,\\
\gamma_i[(k_1+k_2)K+(l_1+l_2)L]&=0,\\
2\gamma_r(K^2+L^2)+2\delta_r(M^4+P^4)+\beta_r(M^2+P^2)&=0,\\
\mathrm{Re}(E)=0,\quad \mathrm{Im}(E)&=0. \qquad \text{(A4)}
\end{aligned}$$

Solving the system of equations (A4) leads to the following cases.

Case 1.1.

$$\gamma_r=0,\quad L=-\frac{K(2k_1\gamma_i+v_g)}{2l_1\gamma_i},\quad l_2=-\frac{l_1(v_g-2k_2\gamma_i)}{2k_1\gamma_i+v_g},$$

$$M=\sqrt{-\frac{\sqrt{\xi_r(\beta_r-\xi_r)}+\beta_r-\xi_r}{2\delta_r}},$$

$$P=\sqrt{\frac{\sqrt{\xi_r(\beta_r-\xi_r)}-\beta_r+\xi_r}{2\delta_r}},$$

$$\chi=-\frac{\beta_r\xi_r+\beta_r^2-2\xi_r^2}{4\delta_r},\quad \delta_i=\frac{\delta_r(\beta_i-\xi_i)}{2(\beta_r-\xi_r)}.$$

In this case, from the above expressions for $|M|$, $|P|$, χ, and δ_i, while keeping all other parameters fixed, we can conclude that as δ_r, the real part of quintic nonlinearity, increases, then $|M|$, $|P|$, and χ, the wave amplitudes and the coefficient of linear gain or loss decrease, and δ_i increases. That is, the quintic nonlinearity puts a damping effect on the linear gain or loss and the wave amplitudes. From the above expressions we conclude in this case that L and K are proportional, and likewise l_1 and l_2. These phenomena are illustrated in Figs. 1–10.

Case 1.2.

$$\gamma_r=0,\quad L=-\frac{K(2k_1\gamma_i+v_g)}{2l_1\gamma_i},\quad M=P,$$

$$P=\sqrt{-\frac{\beta_r}{2\delta_r}},\quad \chi=\frac{-2\beta_r\xi_r-\beta_r^2}{4\delta_r},\quad \xi_i\xi_r=0,$$

We note that as the real part of the coefficient of the quintic term, δ_r, increases, the remaining parameters are fixed, then the value of $|M|$, $|P|$, and χ decrease. This differs from case 1.1 in that the wave amplitudes of M and P are the equal. On the other hand, as β_r, the real part of coefficient of the cubic nonlinearity, increases, so does the linear gain or loss. These phenomena are illustrated in Figs. 1–10.

Case 1.3.

$$\gamma_r=0,\quad P=M,\quad l_2=-l_1,\quad k_2=-k_1,$$

$$M=\sqrt{-\frac{\beta_r}{2\delta_r}},\quad \chi=-\frac{2\beta_r\xi_r+\beta_r^2}{4\delta_r},\quad \xi_i=0,$$

This case is similar to case 1.2, except that K and L are not necessarily proportional, and k_1, k_2, l_1, l_2 are as prescribed here.

Case 1.4.

$$M=P,\quad k_2=-k_1,\quad l_2=l_1=\phi(P,P,k_1),\quad P=\sqrt{\frac{\sqrt{\beta_r^2-8K^2\gamma_r\delta_r}-\beta_r}{4\delta_r}},$$

$$k_1=\frac{\sqrt{2P^2\left[\gamma_i\left(2\gamma_i\xi_i\xi_r+v_g^2\delta_r\right)+\gamma_r\left(2\gamma_i\xi_r^2-v_g^2\delta_i\right)\right]+v_g^2(\gamma_i\beta_r-\beta_i\gamma_r)}-v_g}{4\gamma_i},$$

where the function ϕ is given by (A1). In this case, both continuous waves have the same amplitude, when keeping all other parameters fixed and allowing δ_r to increase, would results in the decrease of the continuous wave amplitudes. On the other hand, if we let the real part of the dispersion coefficient, γ_r to go to zero then the wave amplitudes go to zero too.

Case 1.5.

$$k_2=-k_1,\quad L=0,\quad P=\sqrt{\frac{\sqrt{-16K^2\gamma_r\delta_r-16M^4\delta_r^2-8M^2\beta_r\delta_r+\beta_r^2}-\beta_r}{4\delta_r}}$$

$$l_1=\phi(M,P,k_1),\quad l_2=\phi(P,M,k_1)$$

where the function $\phi(M,P,k_1)$ is given in Eq. (A1) and k_1 is given by the following expression:

$$\begin{aligned}
k_1=-\{v_g[2(M^4+P^4)\delta_r+(M^2+P^2)\beta_r][\beta_i\gamma_i+2(M^2+P^2)(\gamma_i\delta_i+\gamma_r\delta_r)+\beta_r\gamma_r]\}\Big/\Big\{2\Big[\beta_i\Big\{(M^2+P^2)\beta_r\left(\gamma_i^2+\gamma_r^2\right)\\
+2\delta_r\left[\gamma_i^2(M^4+P^4)+(M^2+P^2)^2\gamma_r^2\right]\Big\}+2\delta_i\Big\{\beta_r\left[\gamma_i^2(M^2+P^2)^2+(M^4+P^4)\gamma_r^2\right]\\
+2(M^6+M^4P^2+M^2P^4+P^6)\delta_r\left(\gamma_i^2+\gamma_r^2\right)\Big\}\Big]\Big\},
\end{aligned}$$

and a similar but much longer expression for ξ_i in terms of M, P, and other coefficient parameters. As expected, as δ_r decreases, wave amplitudes increase, as we have seen in other cases.

Case 1.6.

$$l_2 = -l_1, \quad K = 0, \quad M = P,$$
$$k_2^2 = k_1^2, \quad l_1^2 = \phi^2(P,P,k_1),$$
$$P = \sqrt{\frac{4l_1^2\gamma_i(\beta_i\gamma_r - \gamma_i\beta_r)}{8l_1^2\gamma_i(\gamma_i\delta_r - \delta_i\gamma_r) - \xi_r(\gamma_i\xi_i + \gamma_r\xi_r)}},$$
$$L = \sqrt{-\frac{P^2(2P^2\delta_r + \beta_r)}{\gamma_r}}.$$

In this case both continuous-wave amplitudes M and P are the same and as γ_i increases then $|P|$ increases to an asymptotic value given by $\sqrt{\frac{-\beta_r}{8\delta_r}}$. This asymptotic value also shows that as δ_r increases $|P|$ deceases, too. In addition, as γ_r, the real part of dispersion, decreases so does L.

Case 1.7.

$$\gamma_i = 0, \quad l_1 = \phi(M,P,k_1), \quad l_2 = \phi(P,M,k_2),$$
$$L = \sqrt{-\frac{2(K^2\gamma_r + (M^4 + P^4)\delta_r) + (M^2 + P^2)\beta_r}{2\gamma_r}},$$

and solving $\mathrm{Re}E = 0$ and $\mathrm{Im}E = 0$ we obtain two very long expressions for ξ_i and δ_i in terms of M, P, K, k_1, k_2. In this case the solution is valid only for small values of γ_r. Otherwise, as γ_r gets arbitrary large then L is asymptotically given by $\sqrt{-K^2}$ which is not valid since L is a real value.

Case 2. Assume that $C = 0$ but $E \neq 0$. In this case, the dispersion equation is given by

$$\Omega^4 + D\Omega^2 + E\Omega + F = 0,$$

and its roots are given by

$$\Omega_+^{\pm} = \pm\frac{1}{2}\sqrt{-\frac{2E}{q_2} - 2D - q_2^2} + \frac{q_2}{2},$$
$$\Omega_-^{\pm} = \pm\frac{1}{2}\sqrt{\frac{2E}{q_2} - 2D - q_2^2} - \frac{q_2}{2}, \tag{A5}$$

where

$$q_2 = \sqrt{\frac{D^2 + 12F}{3q_1} - \frac{2D}{3} + \frac{q_1}{3}},$$
$$q_1 = 2^{-1/3}\sqrt[3]{q_0 + 2D^3 - 72DF + 27E^2},$$
$$q_0 = \sqrt{(2D^3 - 72DF + 27E^2)^2 - 4(D^2 + 12F)^3}.$$

The above solutions (A5) are valid if $q_1 q_2 \neq 0$. This constraint reduces to $D^2 + 12F \neq 0$ for the existence of solutions in this case. Setting the real and the imaginary parts of $C = 0$, and from the two equations (2.7) and (2.8), we have the following four equations to solve:

$$k_1^2\gamma_r + l_1^2\gamma_r + M^4\delta_r + M^2\beta_r + P^2\xi_r - \chi = 0,$$
$$k_2^2\gamma_r + l_2^2\gamma_r + M^2\xi_r + P^4\delta_r + P^2\beta_r - \chi = 0,$$
$$\gamma_i[(k_1 + k_2)K + (l_1 + l_2)L] = 0,$$
$$2[(K^2 + L^2)\gamma_r + (M^4 + P^4)\delta_r] + (M^2 + P^2)\beta_r = 0.$$

By solving the above system of equations, we obtain the following results described in terms of cases.

Case 2.1.

$$\gamma_i = 0, \quad l_1 = \phi(M,P,k_1), \quad l_2 = \phi(P,M,k_2),$$
$$L = \sqrt{-\frac{2[K^2\gamma_r + (M^4 + P^4)\delta_r] + (M^2 + P^2)\beta_r}{2\gamma_r}}.$$

This case is very similar to case 1.7, thus we expect a similar behavior to occur in gain or loss regions.

Case 2.2.

$$L = 0, \quad k_2 = -k_1, \quad l_1 = l_2 = \phi(P,M,k_1),$$
$$M = \sqrt{\frac{\sqrt{-16\delta_r(K^2\gamma_r + P^4\delta_r) - 8P^2\beta_r\delta_r + \beta_r^2} - \beta_r}{4\delta_r}},$$

where the component continuous-wave vector function $\phi(P,M,k_1)$ is given in Eq. (A1). Here as $|\delta_r|$ increases, the two wave amplitudes asymptotically become equal, i.e., $|M| = |P|$ provided that $\delta_r < 0$ for large values of $|\delta_r|$. This shows in this case that the two waves do not have the same amplitudes for small values of $|\delta_r|$.

Case 2.3.

$$L = -\frac{(k_1 + k_2)K}{l_1 + l_2},$$
$$K = \sqrt{-\frac{(l_1 + l_2)^2[2(M^4 + P^4)\delta_r + (M^2 + P^2)\beta_r]}{2[(k_1 + k_2)^2 + (l_1 + l_2)^2]\gamma_r}},$$
$$l_1 = \phi(M,P,k_1), \quad l_2 = \phi(P,M,k_1).$$

The above solution is valid whenever γ_r is not zero. A decrease in the value of γ_r would result in larger values for $|L|$ and $|K|$.

Since some of these relations are too complicated to analyze analytically, we have performed numerous examples and the results are presented graphically for better illustration. Finally, for case 3, we assume $C \neq 0$ and $E = 0$. The results are similar to case 2, except that the condition for the existence of solutions reduces to $(D^2 + 12F)(C^2 - 4D) \neq 0$. In the case where $\mathrm{Re}E = 0$ and $\mathrm{Im}E = 0$, we have six free parameters and the remaining other parameters are determined as in case 2. The case that requires $CE \neq 0$ was already discussed in Sec. II A.

[1] M. C. Cross and P. C. Hohenberg, Rev. Mod. Phys. **65**, 851 (1993).

[2] I. S. Aranson and L. Kramer, Rev. Mod. Phys. **74**, 99 (2002).

[3] E. L. Rempel, A. C.-L. Chian, A. J. Preto, and S. Stephany, Nonlinear Process. Geophys. **11**, 691 (2004).

[4] N. R. Pereira and L. Stenflo, Phys. Fluids **20**, 1733 (1977).

[5] L. Stenflo, M. Y. Yu, and P. K. Shukla, Phys. Scr. **40**, 257 (1989).

[6] L. C. Crasovan, B. A. Malomed, D. Mihalache, D. Mazilu, and F. Lederer, Phys. Rev. E **62**, 1322 (2000).
[7] P. Kolodner, Phys. Rev. A **44**, 6448 (1991).
[8] P. A. Belanger, L. Gagnon, and C. Paré, Opt. Lett. **14**, 943 (1989).
[9] Y. Kuramoto, *Chemical Oscillations, Waves and Turbulence* (Springer-Verlag, Berlin, 1984).
[10] A. C. Newell and J. V. Moloney, *Nonlinear Optics* (Addison-Wesley, Reading, MA, 1992).
[11] C. Normand and Y. Pomeau, Rev. Mod. Phys. **49**, 581 (1977).
[12] S. Rasenat, V. Steinberg, and I. Rehberg, Phys. Rev. A **42**, 5998 (1990).
[13] F. Ndzana, A. Mohamadou, and T. C. Kofané, Phys. Rev. E **79**, 056611 (2009).
[14] K. Nozaki and N. Bekki, J. Phys. Soc. Jpn. **53**, 1581 (1984).
[15] J. M. Weiss, M. Tabor, and G. Carnevale, J. Math. Phys. **24**, 522 (1983).
[16] R. Conte and M. Musette, Physica D **69**, 1 (1993).
[17] R. J. Deissler and H. R. Brand, Phys. Rev. Lett. **81**, 3856 (1998).
[18] H. Tian, Z. Li, J. Tian, and G. Zhou, Phys. Rev. E **66**, 066204 (2002).
[19] W. van Saarloos and P. C. Hohenberg, Physica D **56**, 303 (1992).
[20] R. J. Deissler and H. R. Brand, Phys. Lett. A **146**, 252 (1990).
[21] A. Mohamadou, B. E. Ayissi, and T. C. Kofané, Phys. Rev. E **74**, 046604 (2006).
[22] A. J. Lichtenberg and M. A. Liberman, *Regular and Stochastic Motion* (Springer-Verlag, New York, 1983).
[23] E. Ott, *Chaos in Dynamical Systems* (Cambridge University, Cambridge, England, 1993).
[24] C. T. Zhou, C. H. Lai, and M. Y. Yu, Phys. Scr. **55**, 394 (1997); J. Math. Phys. **38**, 5225 (1997).
[25] C. Sulem and P. L. Sulem, *The Nonlinear Schrödinger Equation: Self-Focusing and Wave Collapse* (Springer, New York, 1999).
[26] G. P. Agrawal, *Nonlinear Fiber Optics* (Academic, San Diego, 2001).
[27] E. Kengne, J. Phys. A **37**, 6053 (2004).
[28] F. B. Pelap, T. C. Kofané, N. Flytzanis, and M. Remoissenet, J. Phys. Soc. Jpn. **70**, 2568 (2001).
[29] E. Kengne, S. T. Chui, and W. M. Liu, Phys. Rev. E **74**, 036614 (2006).
[30] M. Onorato, A. R. Osborne, M. Serio, and S. Bertone, Phys. Rev. Lett. **86**, 5831 (2001).
[31] I. I. Didenkulova, I. F. Nikolkina, and E. N. Pelinovsky, JETP Lett. **97**, 194 (2013).
[32] P. G. Kevrekidis, R. Carretero-González, G. Theocharis, D. J. Frantzeskakis, and B. A. Malomed, Phys. Rev. A **68**, 035602 (2003).
[33] K. Kasamatsu and M. Tsubota, Phys. Rev. A **74**, 013617 (2006).
[34] D. I. Choi and Q. Niu, Phys. Rev. Lett. **82**, 2022 (1999).
[35] C. Orzel, A. K. Tuchman, M. L. Fenselau, M. Yasuda, and M. Kasevich, Science **291**, 2386 (2001).
[36] K. Burnett, M. Edwards, C. W. Clark, and M. Shotter, J. Phys. B **35**, 1617 (2002).
[37] W. P. Hong, Z. Naturforsch **61**, 225 (2006).
[38] A. Mohamadou, C. G. Latchio Tiofack, and T. C. Kofané, Phys. Rev. E **82**, 016601 (2010).
[39] M. Saha and A. K. Sarma, Opt. Comm. **291**, 321 (2013).
[40] R. Sabry, W. M. Moslem, and P. K. Shukla, Phys. Rev. E **86**, 036408 (2012).
[41] C. G. Latchio Tiofack, A. Mohamadou, T. C. Kofané, and A. B. Moubissi, Phys. Rev. E **80**, 066604 (2009).
[42] Y. Xiang, S. Wen, X. Dai, and D. Fan, Phys. Rev. E **82**, 056605 (2010).
[43] J. M. Alcaraz-Pelegrina and P. Rodríguez-García, Phys. Lett. A **374**, 1591 (2010).
[44] R. J. Deissler and H. R. Brand, Phys. Rev. A **44**, R3411 (1991).
[45] L. Ge, M. Shen, T. Zang, C. Ma, and L. Dai, Phys. Rev. E **91**, 023203 (2015).
[46] M. van Hecke, Phys. Rev. Lett. **80**, 1896 (1998).
[47] L. Brusch, M. G. Zimmermann, M. van Hecke, M. Bär, and A. Torcini, Phys. Rev. Lett. **85**, 86 (2000).
[48] C. Cartes, O. Descalzi, and H. R. Brand, Phys. Rev. E **85**, 015205 (2012).
[49] O. Descalzi, C. Cartes, J. Cisternas, and H. R. Brand, Phys. Rev. E **83**, 056214 (2011).
[50] M. Ipsen and P. G. Sorensen, Phys. Rev. Lett. **84**, 2389 (2000).
[51] G.-A. Zakeri and E. Yomba, Phys. Scr. **88**, 025006 (2013).